Inorg. Chem. **2003**, *42*, 8663–8673

Substituent and Isomer Effects on Structural, Spectroscopic, and Electrochemical Properties of Dirhodium(III,II) Complexes Containing Four Identical Unsymmetrical Bridging Ligands

Karl M. Kadish,*,† Tuan D. Phan,† Lingamallu Giribabu,† Eric Van Caemelbecke,†,‡ and John L. Bear*,†

Departments of Chemistry, University of Houston, Houston, Texas 77204-5003, and Houston Baptist University, Houston, Texas 77074-3298

Received August 12, 2003

Substituent and isomer effects on the structural, spectroscopic, (UV–visible and ESR) and electrochemical properties of dirhodium(III,II) complexes containing four identical unsymmetrical bridging ligands are reported for seven related compounds of the type $Rh_2(L)_4Cl$ where L = 2-(2-fluoroanilino)pyridinate (2-Fap), 2-(2,6-difluoroanilino)pyridinate (2,6-F_2ap), 2-(2,4,6-trifluoroanilino)pyridinate (2,4,6-F_3ap), or 2-(2,3,4,5,6-pentafluoroanilino)pyridinate (F_5ap) anion. Rh_2(2-Fap)$_4$Cl exists only in a (4,0) isomeric conformation while Rh_2(2,6-F_2ap)$_4$Cl, Rh_2(2,4,6-F_3ap)$_4$Cl, and Rh_2-(F_5ap)$_4$Cl exist as both (4,0) and (3,1) isomers. It had earlier been demonstrated that $Rh_2(L)_4Cl$ complexes can adopt different geometric conformations of the bridging ligands, but the current study provides the first example where two geometric isomers of Rh_2^{5+} complexes are obtained for one compound using the same synthetic procedure. The synthesis, structural, spectroscopic, and/or electrochemical properties of (3,1) Rh_2(2,6-F_2ap)$_4$CN and (4,0) Rh_2(2,4,6-F_3ap)$_4$(C≡C)$_2$Si(CH$_3$)$_3$ are also reported and the data on these compounds is discussed in light of their parent complexes, (3,1) Rh_2(2,6-F_2ap)$_4$Cl and (4,0) Rh_2(2,4,6-F_3ap)$_4$Cl.

Introduction

A large number of tetracarboxylate-type complexes containing Rh_2 or Ru_2 cores have been synthesized and characterized by structural, electrochemical, and spectroscopic methods.[1−23] Among these, compounds with four unsymmetrical bridging ligands, such as in the case of the 2-anilinopyridinate anion, can theoretically exhibit four modes of bridging symmetry around the dimetal core which are designated as (4,0), (3,1), (2,2)-trans, and (2,2)-cis geometric isomers. Examples have been reported in the literature for Rh_2^{4+} and Rh_2^{5+} species with (4,0), (3,1), and (2,2)-trans isomeric forms,[3,4,24] but to date the possibility of

* Authors to whom correspondence should be addressed. E-mail: kkadish@uh.edu (K.M.K.).
† University of Houston.
‡ Houston Baptist University.

(1) Stephenson, T. A.; Wilkinson, G. *J. Inorg. Nucl. Chem.* **1966**, *28*, 2285.
(2) Chakravarty, A. R.; Cotton, F. A.; Tocher, D. A. *Inorg. Chem.* **1985**, *24*, 172.
(3) Bear, J. L.; Liu, L. M.; Kadish, K. M. *Inorg. Chem.* **1987**, *26*, 2927.
(4) Bear, J. L.; Yao, C. L.; Liu, L. M.; Capdevielle, F. J.; Korp, J. D.; Albright, T. A.; Kang, S. K.; Kadish, K. M. *Inorg. Chem.* **1989**, *28*, 1254.
(5) Yao, C. L.; Park, K. H.; Khokhar, A. R.; Jun, M. J.; Bear, J. L. *Inorg. Chem.* **1990**, *29*, 4033.
(6) Cotton, F. A.; Walton, R. A. *Multiple Bonds Between Metal Atoms*; Oxford University Press: Oxford, 1993.
(7) Bear, J. L.; Li, Y.; Han, B.; Van Caemelbecke, E.; Kadish, K. M. *Inorg. Chem.* **1997**, *36*, 5449.
(8) Aquino, M. A. S. *Coord. Chem. Rev.* **1998**, *170*, 141.
(9) Bear, J. L.; Wellhoff, J.; Royal, G.; Van Caemelbecke, E.; Eapen, S.; Kadish, K. M. *Inorg. Chem.* **2001**, *40*, 2282.
(10) Bear, J. L.; Han, B.; Wu, Z.; Van Caemelbecke, E.; Kadish, K. M. *Inorg. Chem.* **2001**, *40*, 2275.
(11) Kadish, K. M.; Wang, L.-L.; Thuriere, A.; Van Caemelbecke, E.; Bear, J. L. *Inorg. Chem.* **2003**, *42*, 834.
(12) Connelly, N. G.; Davis, P. R. G.; Harry, E. E.; Klangsinsirukul, P.; Venter, M. *J. Chem. Soc., Dalton Trans.* **2000**, 2273.
(13) Zhang, G.; Zhao, J.; Raudaschl-Sieber, G.; Herdtweck, E.; Kuhn, F. E. *Polyhedron* **2002**, *21*, 1737.
(14) Handa, M.; Muraki, Y.; Mikuriya, M.; Azuma, H.; Kasuga, K. *Bull Chem. Soc. Jpn.* **2002**, *75*, 1755.
(15) Sayama, Y.; Handa, M.; Mikuriya, M.; Hiromitsu, I.; Kasuga, K. *Bull Chem. Soc. Jpn.* **2003**, *76*, 769.
(16) Zuo, J. L.; Biani, F. F.; Santos, A. M.; Kohler, K.; Kuhn, F. E. *Eur. J. Inorg. Chem.* **2003**, 449.
(17) Sorasaenee, K.; Galan-Mascaros, J. R.; Dunbar, K. R. *Inorg. Chem.* **2003**, *42*, 661.
(18) Xu, G.-L.; Jablonski, C. G.; Ren, T. *Inorg. Chim. Acta* **2003**, *343*, 387.
(19) Xu, G.-L.; Zou, G.; Ni, Y.-H.; DeRosa, M. C.; Crutchley, R. J.; Ren, T. *J. Am. Chem. Soc.* **2003**, *125*, 10057.
(20) Chisholm, M. H. *Acc. Chem. Res.* **2000**, *33*, 53.
(21) Ren, T. *Coord. Chem. Rev.* **1998**, *175*, 43.
(22) Eglin, J. L.; Lin, C.; Ren, T.; Smith, L.; Staples, R. J.; Wipf, D. O. *Eur. J. Inorg. Chem.* **1999**, 2095.
(23) Ren, T.; Lin, C.; Valente, E. J.; Zubkowski, J. D. *Inorg. Chim. Acta* **2000**, *297*, 283.

10.1021/ic034963l CCC: $25.00
Published on Web 11/27/2003

Chart 1

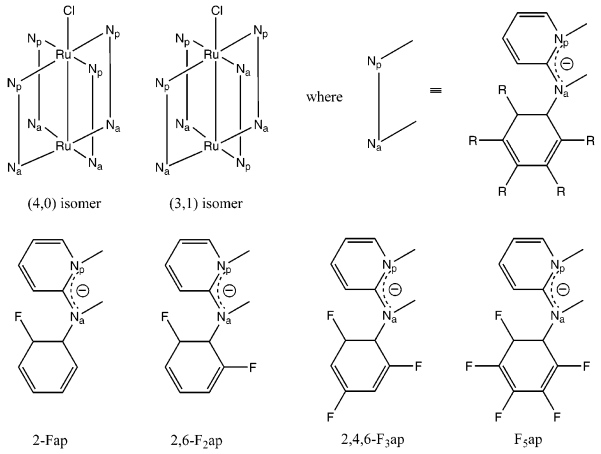

forming more than one geometric isomer using exactly the same experimental procedure has been limited exclusively to tetracarboxylate-type complexes with a Ru_2^{5+} core.[11]

Previously synthesized $Ru_2(L)_4Cl$ complexes, where L = ap, 2-CH_3ap, 2-Fap, 2,5-F_2ap, 2,6-F_2ap, 2,4,6-F_3ap, or F_5ap, have been shown to possess an isomeric distribution which depends upon the substitution of the ap (2-anilinopyridinate) ligand. In addition, for a given bridging ligand, the Ru_2^{5+} complexes were isolated from the same reaction mixture in one, two, or three different isomeric forms.[2,7,9,11] These earlier studies suggested that both electronic and steric effects may be responsible for the preferred isomeric binding mode of the bridging ligand on Ru_2^{5+}. The type of dimetal core may also govern the isomeric distribution, and this possibility prompted us to synthesize a series of substituted ap derivatives containing a Rh_2^{5+} core and bridging ligands identical to those which have been examined in the diruthenium(III,II) series of compounds.[11] A schematic representation of the substituted 2-anilinopyridinate compounds investigated in this present manuscript is given in Chart 1 where the bridging ligands differ in the number and position of fluorine atoms on the phenyl group of the anilinopyridinate anion. These compounds were investigated in the present paper with respect to their structural, spectroscopic, and electrochemical properties.

It has been shown that dirhodium(III,II) derivatives will axially bind a variety of neutral and anionic ligands, and several crystal structures of these compounds containing one or two axially coordinated ligands are known.[4−6,10,25−30] The Rh−Rh bond lengths as well as the electrochemical properties of dirhodium(III,II) compounds having four identical bridging ligands are known to be affected by the mode of axial ligation,[4,5] and we have therefore in the present study also compared the structural, electrochemical, and spectroscopic properties of (3,1) Rh_2(2,6-F_2ap)$_4$CN and (4,0) Rh_2(2,4,6-F_3ap)$_4$(C≡C)$_2$Si(CH_3)$_3$ to their parent complexes (3,1) Rh_2(2,6-F_2ap)$_4$Cl and (4,0) Rh_2(2,4,6-F_3ap)$_4$Cl, respectively.

Experimental Section

Chemicals and Reagents. Ultrahigh-purity argon (99.999% min) and high-purity nitrogen were purchased from Matheson-Trigas Co. and were passed through anhydrous calcium sulfate and potassium hydroxide pellets to remove trace oxygen and water prior to use. GR grade dichloromethane, acetonitrile, hexanes, methanol, absolute dichloromethane (Fluka) for electrochemical measurements, and absolute ethyl alcohol (McCormick, Inc.) for recrystallization were used without purification. Tetra-*n*-butylammonium perchlorate (TBAP) was purchased from Fluka Chemical Co., twice recrystallized from ethyl alcohol, and stored in a vacuum oven at 40 °C for at least 1 week prior to use. Tetra-*n*-butylammonium chloride (TBACl) and tetra-*n*-butylammonium cyanide (TBACN) were purchased from Fluka Chemical Co. and used as received. 2-Bromopyridine (C_5H_4NBr), 2-fluoroaniline ($C_6H_4FNH_2$), 2,6-difluoroaniline ($C_6H_3F_2NH_2$), 2,4,6-trifluoroaniline ($C_6H_2F_3NH_2$), 2,3,4,5,6-pentafluoroaniline ($C_6F_5NH_2$), 1,4-bis(trimethylsilyl)-1,3-butadiyne ($C_{10}H_{18}Si_2$), anhydrous tetrahydrofuran (99.9%), and carbon tetrachloride (CCl_4) were purchased from Aldrich Co. and used as received. Tetrakis(μ-acetato)dirhodium(II) ($Rh_2(O_2CCH_3)_4$) was purchased from Strem Chemical Co. and used without further purification. Silica gel (Merck 230−400 mesh 60 Å) used for column chromatography was purchased from Aldrich Co.

Physical Measurements. Cyclic voltammetry was carried out with an EG&G model 173 potentiostat. A three electrode system was used and consisted of a glassy carbon working electrode, a platinum wire counter electrode, and a homemade saturated calomel electrode (SCE) as the reference electrode. The SCE was separated from the bulk of the solution by a fritted-glass bridge of low porosity that contained the solvent/supporting electrolyte mixture. All potentials are referenced to the SCE, and all measurements were carried out at room temperature.

Spectroelectrochemical experiments were performed using an EG&G model 173 potentiostat and a thin-layer cell whose design has been described in the literature.[31] Time-resolved UV−visible spectra were recorded with a Hewlett-Packard model 8453 diode array spectrophotometer.

Mass spectra were recorded on an Applied Biosystem Voyager DE-STR MALDI-TOF mass spectrometer equipped with a nitrogen laser (337 nm) at the University of Houston Mass Spectrometry Laboratory. ESR spectra were recorded at 77 K in CH_2Cl_2/CH_3CN with a modified Varian E-4 ESR spectrometer, which was interfaced to a tracor Northern TN-1710 signal averager. Elemental analyses were carried out by Atlantic Microlab, Inc., Norcross, GA.

The effective magnetic moments were determined by the Evans method[32] using a General Electric QE-300 FT NMR spectrometer with CD_2Cl_2 as solvent and TMS as the internal reference. IR spectra were recorded on a ThermoNicolet Avatar 370-FT-IR spectrometer.

(24) Takashi, K.; Hisanori, K.; Hiroshi, F.; Chihiro, K. T.; Yuzuru, K.; Naohiro, K.; Masahiro, E.; Kunihisa, S.; Takayoshi, K. S.; Megumu, M. *Bull Chem. Soc. Jpn.* **2000**, *73*, 657.
(25) Bear, J. L.; Lifsey, R. S.; Chau, L. K.; Ahsan, M. Q.; Korp, J. D.; Chavan, M.; Kadish, K. M. *J. Chem. Soc., Dalton Trans.* **1989**, 93−100.
(26) Ziolkowski, J. J.; Moszner, M.; Glowiak, T. *J. Chem. Soc., Chem. Commun.* **1977**, 760.
(27) Piraino, P.; Bruno, G.; Nicolo, F.; Faraone, F.; Schiavo, S. L. *Inorg. Chem.* **1985**, *24*, 4760.
(28) Aoki, K.; Hoshino, M.; Okada, T.; Yamazaki, H.; Sekizawa, H. *J. Chem. Soc., Chem. Commun*. **1986**, 314.
(29) Baranovskii, I. B.; Golubnichaya, L. M.; Rotov, A. V.; Shchelokov, R. N.; Porai-Koshits, M. A. *Russ. J. Inorg. Chem.* **1986**, *31*, 1652.
(30) Bear, J. L.; Yao, C. L.; Lifsey, R. S.; Korp, J. D.; Kadish, K. M. *Inorg. Chem*. **1991**, *30*, 336.
(31) Lin, X. Q.; Kadish, K. M. *Anal. Chem*. **1985**, *57*, 1498.
(32) Evans, D. F. *J. Chem. Soc.* **1959**, 2003.

Synthesis. Tetrakis(trifluoroacetato)dirhodium(II) $Rh_2(O_2CCF_3)_4$,[33] H(2-Fap), H(2,6-F_2ap), H(2,4,6-F_3ap), and H(2,3,4,5,6-F_5ap)[34] were synthesized following methods described in the literature.

All seven compounds **1**−**7** were synthesized in a manner similar to what has been described for (4,0) $Rh_2(ap)_4Cl$.[10] The general procedure is given below for (4,0) Rh_2(2-Fap)$_4$Cl (**1**).

(4,0) Rh_2(2-Fap)$_4$Cl (1). $Rh_2(O_2CCF_3)_4$ (0.2 g, 0.30 mmol) and a large excess of H(2-Fap) (1.8 g, 9.6 mmol) were mixed in toluene and refluxed at 120 °C for 24 h. The solvent was removed using a rotary evaporator. The remaining residue was dissolved in CH_2Cl_2 containing 30% CCl_4 (v/v) and left to stand for 4 h in sunlight to generate Rh_2(2-Fap)$_4$Cl. The solvent was removed by rotary evaporation, and the residue was sublimed under vacuum at 110 °C to remove excess H(2-Fap) ligand. The remaining solid was subjected to silica gel column chromatography using a CH_2Cl_2/hexanes (9/1, v/v) solvent mixture as eluent. Only one red band was observed on the column. After evaporation of the eluent, the title compound was recovered in a 60% yield. Mass spectral data [*m*/*e*, (fragment)]: 989, $[Rh_2(2\text{-Fap})_4Cl]^+$; 954, $[Rh_2(2\text{-Fap})_4]^+$. Anal. Calcd for $C_{44}H_{32}N_8F_4ClRh_2$: C, 53.33; H, 3.23; N, 11.31; F, 7.67. Found: C, 53.21; H, 3.29; N, 11.40; F, 7.59. UV−vis spectrum in CH_2Cl_2 [λ_{max}, nm (10^{-3} ϵ, mol^{-1} L cm^{-1})]: 497 (3.5), 559 (2.6), 920 (5.1).

(4,0) Rh_2(2,6-F_2ap)$_4$Cl (2) and (3,1) Rh_2(2,6-F_2ap)$_4$Cl (3). Two red bands of Rh_2(2,6-F_2ap)$_4$Cl were observed on the column. The first band collected was the (4,0) isomer and the second the (3,1) isomer. The yields were 25% for the (4,0) isomer and 30% for the (3,1) isomer. Mass spectral data [*m*/*e*, (fragment)] of the (4,0) and (3,1) isomers: 1061, $[Rh_2(2,6\text{-}F_2ap)_4Cl]^+$; 1026, $[Rh_2(2,6\text{-}F_2ap)_4]^+$. Anal. Calcd for $C_{44}H_{28}N_8F_8ClRh_2$ of the (4,0) and (3,1) isomers: C, 49.75; H, 2.64; N, 10.55; F, 14.32. Found: C, 49.79; H, 2.65; N, 10.53; F, 14.29. UV−vis spectrum in CH_2Cl_2 [λ_{max}, nm (10^{-3} ϵ, mol^{-1} L cm^{-1})] (4,0) isomer: 505 (3.4), 561 (sh), 718 (0.5), 977 (3.8); (3,1) isomer: 517 (2.8), 542 (2.8), 695 (1.2), 1004 (5.0).

(4,0) Rh_2(2,4,6-F_3ap)$_4$Cl (4) and (3,1) Rh_2(2,4,6-F_3ap)$_4$Cl (5). Two red bands of Rh_2(2,4,6-F_3ap)$_4$Cl were observed and collected from the column. The first band corresponded to the (4,0) isomer and the second to the (3,1) isomer. Attempts to grow suitable crystals for X-ray crystallography were not successful for either isomer. However, the Rh_2^{5+} compound in the first band was assigned as having a (4,0) isomeric conformation on the basis of its similarity in properties to Rh_2(2,4,6-F_3ap)$_4$(C≡C)$_2$Si(CH_3)$_3$, which was structurally characterized in the present study. The Rh_2^{5+} compound in the second band was assigned as the (3,1) isomer on the basis of its UV−vis spectral features (see following sections of manuscript). The yields were 18% for the proposed (4,0) isomer and 27% for the proposed (3,1) isomer. Mass spectral data [*m*/*e*, (fragment)] of the (4,0) and (3,1) isomers: 1133, $[Rh_2(2,4,6\text{-}F_2ap)_4Cl]^+$; 1089, $[Rh_2(2,4,6\text{-}F_2ap)_4]^+$. Anal. Calcd for $C_{44}H_{24}N_8F_{12}ClRh_2$ of the (4,0) and (3,1) isomers: C, 46.68; H, 2.12; N, 9.90; F, 20.16. Found: C, 46.75; H, 2.11; N, 9.81; F, 19.99. UV−vis spectrum in CH_2Cl_2 [λ_{max}, nm (10^{-3} ϵ, mol^{-1} L cm^{-1})] (4,0) isomer: 500 (3.7), 561 (sh), 711 (0.6), 990 (3.8); (3,1) isomer: 512 (2.9), 542 (2.9), 692 (0.9), 1000 (5.4).

(4,0) Rh_2(F_5ap)$_4$Cl (6) and (3,1) Rh_2(F_5ap)$_4$Cl (7). Two red bands of Rh_2(F_5ap)$_4$Cl were observed on the column. All attempts to grow suitable crystals of the compound in the first fraction for X-ray crystallography were not successful. However, this compound was assigned as having a (4,0) isomeric form on the basis of its UV−vis spectral features (see following sections). An X-ray structure reveals that the compound in the second fraction was the (3,1) isomer of Rh_2(F_5ap)$_4$Cl. The yields were 10% for the proposed (4,0) isomer and 20% for the structurally characterized (3,1) isomer. Mass spectral data [*m*/*e*, (fragment)] of the (4,0) and (3,1) isomers: 1275, $[Rh_2(F_5ap)_4Cl]^+$; 1241, $[Rh_2(F_5ap)_4]^+$. Anal. Calcd for $C_{44}H_{16}N_8F_{20}ClRh_2$ of the (4,0) and (3,1) isomers: C, 41.41; H, 1.25; N, 8.78; F, 29.89. Found: C, 41.50; H, 1.21; N, 8.68; F, 29.28. UV−vis spectrum in CH_2Cl_2 [λ_{max}, nm (10^{-3} ϵ, mol^{-1} L cm^{-1})] (4,0) isomer: 535 (sh), 542 (2.3), 700 (0.6), 1009 (3.7); (3,1) isomer: 549 (2.7), 580 (2.9), 688 (0.9), 1029 (4.4).

(3,1) Rh_2(2,6-F_2ap)$_4$CN (8). A mixture of the (3,1) isomer of Rh_2(2,6-F_2ap)$_4$Cl (100 mg, 0.0974 mmol) and NaCN (47.7 mg, 0.9740 mmol) was dissolved in CH_2Cl_2 and refluxed for 10 h, during which time the color of the solution changed from red to green. The reaction mixture was then extracted with water to remove any excess NaCN. The green colored organic layer was collected and the solvent was evaporated. The crude product was subjected to a silica gel column using CH_2Cl_2 as eluent. Two fractions were observed on the column, one red and the other green. These were collected as the starting material and the (3,1) isomer of Rh_2(2,6-F_2ap)$_4$CN, respectively. The yield was 95% for (3,1) Rh_2(2,6-F_2ap)$_4$CN. Mass spectral data [*m*/*e*, (fragment)]: 1051, $[Rh_2(2,6\text{-}F_2ap)_4CN]^+$; 1026, $[Rh_2(2,6\text{-}F_2ap)_4]^+$. Anal. Calcd for $C_{45}H_{28}N_9F_8Rh_2$: C, 51.40; H, 2.66; N, 11.98; F, 14.46. Found: C, 51.78; H, 2.70; N, 11.80; F, 14.30. IR (cm^{-1}): 2110 [ν(C≡N)]. UV−vis spectrum data in CH_2Cl_2: [λ_{max}, nm (ϵ x 10^{-3}, M^{-1} cm^{-1}): 433 (2.4), 478 (1.9), 648 (1.1), 862 (4.2).

(4,0) Rh_2(2,4,6-F_3ap)$_4$(C≡C)$_2$Si(CH_3)$_3$ (9). This complex was prepared following a method described by Bear et al.[10] Typically, a solution of dry THF containing Li(C≡C)$_2$Si(CH_3)$_3$ (0.25 g, 2.4 mmol) was added to a dry THF solution of (4,0) Rh_2(F_3ap)$_4$Cl (0.10 g, 0.08 mmol) under an argon atmosphere, and the mixture was refluxed under argon for 24 h. The color of the solution changed progressively from red to red-brown during reflux. The solvent was evaporated, and the residue was subjected to silica gel column chromatography using CH_2Cl_2 as eluent. Two bands were observed on the column, one red and the other red-brown. These were collected as the starting material and the (4,0) isomer of Rh_2(2,4,6-F_3ap)$_4$(C≡C)$_2$Si(CH_3)$_3$, respectively. The yield was 90% for the (4,0) isomer of Rh_2(2,4,6-F_3ap)$_4$(C≡C)$_2$Si(CH_3)$_3$. Mass spectral data [*m*/*e*, (fragment)]: 1119, $[Rh_2(2,4,6\text{-}F_3ap)_4(C{\equiv}C)_2Si(CH_3)_3]^+$; 1098, $[Rh_2(2,4,6\text{-}F_3ap)_4]^+$. Anal. Calcd for $C_{54}H_{40}N_8F_{12}SiRh_2$: C, 50.21; H, 2.71; N, 9.19; F, 18.70. Found: C, 51.05; H, 2.81; N, 9.23; F, 18.48. IR (cm^{-1}): 2168, 2139, 2123 [ν(C≡C)]. UV−vis spectrum data in CH_2Cl_2: [λ_{max}, nm (ϵ × 10^{-3}, M^{-1} cm^{-1}): 460 (4.2), 547 (4.0), 878 (7.8).

X-ray Crystallography of Compounds 1−3 and 7−9. Single-crystal X-ray crystallographic studies were performed at the University of Houston X-ray Crystallographic Center. Each sample was placed in a steam of dry nitrogen gas at −50 °C in a random position. The radiation used was Mo Kα monochromatized by a highly ordered graphite crystal. Final cell constants as well as other information pertinent to data collection and structure refinement are listed in Tables 1 and 2.

All measurements were made with a Siemens SMART platform diffractometer equipped with a 1K CCD area detector. A hemisphere of data 1271 frames at 5 cm detector distance was collected using a narrow-frame method with scan widths of 0.30° ω and an exposure time of 30 s/frame. The first 50 frames were measured again at the end of data collection to monitor instrument and crystal stability, and the maximum correction on *I* was <1%. The data were integrated using the Siemens SAINT program, with the

(33) Telser, J.; Drago, R. S. *Inorg. Chem.* **1984**, *23*, 2599.
(34) Hisano, T.; Matsuoka, T.; Tsutsumi, K.; Muraoka, K.; Ichikawa, M. *Chem. Pharm. Bull.* **1981**, *29*, 3706.

Table 1. Crystal Data and Data Collection and Processing Parameters for the (4,0) Isomers of the Characterized Compounds

	(4,0) isomer		
	Rh_2(2-Fap)$_4$Cl (**1**)	Rh_2(2,6-F_2ap)$_4$Cl (**2**)	Rh_2(2,4,6-F_3ap)$_4$-(C≡C)$_2$Si(CH$_3$)$_3$ (**9**)
space group	*P*4*nc* tetragonal	*C*2/*c* monoclinic	$P\bar{1}$ triclinic
cell constant			
a (Å)	15.2139(8)	19.4773(10)	10.734(1)
b (Å)	15.2139(8)	15.0962(7)	14.427(2)
c (Å)	9.6116(7)	16.9620(8)	18.894(2)
α (deg)	90	90.0	74.111(2)
β (deg)	90	109.245(1)	74.702(2)
γ (deg)	90	90	81.555(2)
V (Å^3)	2224.7(2)	4708.7(4)	2705.4(6)
mol formula	$C_{44}H_{32}N_8F_4Cl$-Rh_2·2CH_2Cl_2	$C_{44}H_{28}N_8F_8Cl$-Rh_2·2CH_2Cl_2	$C_{51}H_{33}N_8F_{12}$-$SiRh_2$
fw (g/mol)	1159.90	1231.87	1262.85
Z	2	4	2
ρ_{calcd} (g/cm^3)	1.731	1.738	1.550
μ (cm^{-1})	1.104	1.061	0.720
λ(Mo Kα) (Å)	0.71073	0.71073	0.71073
temp (K)	223	223	223
R (F_o)[a]	0.0207	0.0399	0.0764
R_w (F_o)[b]	0.0480	0.1006	0.1910

[a] $R = \sum||F_o| - |F_c||/\sum|F_o|$. [b] $R_w = [\sum_w(|F_o| - |F_c|)^2/\sum_w|F_o|^2]^{1/2}$.

Table 2. Crystal Data and Data Collection and Processing Parameters for the (3,1) Isomers of the Characterized Compounds

	(3,1) isomer		
	Rh_2(2,6-F_2ap)$_4$Cl (**3**)	Rh_2(F_5ap)$_4$Cl (**7**)	Rh_2(2,6-F_2ap)$_4$CN (**8**)
space group	*P*2$_1$/*n* monoclinic	*P*2$_1$/*c* monoclinic	*P*2$_1$/*n* monoclinic
cell constant			
a (Å)	12.8179(6)	15.3722(8)	13.0374(16)
b (Å)	23.5726(12)	14.0987(7)	23.6332(29)
c (Å)	15.2275(8)	26.2826(14)	15.2597(19)
α (deg)	90	90	90
β (deg)	93.422(1)	106.025	94.187(2)
γ (deg)	90	90	90
V (Å^3)	4592.8(4)	5474.8(5)	4689.2(10)
mol formula	$C_{44}H_{28}N_8F_8Cl$-Rh_2·2CH_2Cl_2	$C_{44}H_{16}N_8F_{20}Cl$-Rh_2·2CH_2Cl_2	$C_{45}H_{28}N_9F_8$-Rh_2·2CH_2Cl_2
fw (g/mol)	1231.87	1447.77	1222.44
Z	4	4	4
ρ_{calcd} (g/cm^3)	1.782	1.756	1.732
μ (cm^{-1})	1.088	0.957	1.010
λ(Mo Kα) (Å)	0.71073	0.71073	0.71073
temp (K)	223	223	223
R (F_o)[a]	0.0335	0.0385	0.0377
R_w (F_o)[b]	0.0932	0.1029	0.1023

[a] $R = \sum||F_o| - |F_c||/\sum|F_o|$. [b] $R_w = [\sum w(|F_o| - |F_c|)^2/\sum w|F_o|^2]^{1/2}$.

intensities corrected for Lorentz factor, polarization, air absorption, and absorption due to variation in the path length through the dectector faceplate. A Ψ-scan absorption correction was applied based on the entire data set. Redundant reflections were averaged. Final cell constants were refined using 4116 reflections for **1**, 5606 reflections for **2**, 6747 reflections for **3**, 5591 reflections for **7**, 6781 reflections for **8**, and 4092 reflections for **9** having $I > 10\sigma(I)$. The Laue symmetry was determined to be 4/*mmm* for **1** and 2/*m* for **2**, **3**, **7**, and **8**, and −1 for **9** from the systematic absences noted; the space groups were shown to be *P*4*nc* for **1,** *C*2/*c* for **2**, *P*2$_1$/*n* for **3** and **8**, *P*2$_1$/*c* for **7**, and $P\bar{1}$ for **9**.

Results and Discussion

Seven dirhodium complexes having the structural type Rh_2(L)$_4$Cl, where L is the monoanion 2-Fap, 2,6-F_2ap, 2,4,6-F_3ap, or F_5ap, were synthesized according to eq 1 and characterized with respect to their electrochemical, spectroscopic, and structural properties.

$$Rh_2(CF_3CO_2)_4 + 4HL \xrightarrow[2.\ CH_2Cl_2/CCl_4]{1.\ \text{toluene}} Rh_2(L)_4Cl + 4CF_3CO_2H \quad (1)$$
$$3.\ \text{light}$$

As described in the Experimental Section, the synthesis of Rh_2(L)$_4$Cl was carried out in refluxing toluene for 24 h. The excess ligand was removed by sublimation and the product purified by column chromatography. The title compounds were recovered in overall yields (both isomers) which ranged from 30% to 60%. The yield and isomeric distribution did not depend on the time the reaction was carried out, and similar results were obtained whether the mixture was left to react for 16 or 32 h.

(3,1) Rh_2(2,6-F_2ap)$_4$CN was prepared by a reaction between the (3,1) isomer of Rh_2(2,6-F_2ap)$_4$Cl and sodium cyanide according to eq 2.

$$Rh_2(2,6\text{-}F_2ap)_4Cl + NaCN \rightarrow Rh_2(2,6\text{-}F_2ap)_4CN + NaCl \quad (2)$$

As described in the Experimental Section, the synthesis of the (3,1) isomer of Rh_2(2,6-F_2ap)$_4$CN was carried out in refluxing dichloromethane for 10 h. Excess sodium cyanide was extracted with water and the product purified by column chromatography. The cyano complex was obtained in 90% yield. Only the monoadduct, (3,1) Rh_2(2,6-F_2ap)$_4$CN, was recovered when the mixture was left to react for 5 or 20 h.

The (4,0) isomer of Rh_2(2,4,6-F_3ap)$_4$(C≡C)$_2$Si(CH$_3$)$_3$ was obtained by treating the (4,0) isomer of Rh_2(2,4,6-F_3ap)$_4$Cl with excess Li(C≡C)$_2$Si(CH$_3$)$_3$ in dry THF. For isomeric identification purposes, only the X-ray structure of this complex was determined.

On the basis of the combined structural, spectroscopic, and electrochemical data (described below), the complex with the four 2-Fap bridging ligands is shown to exist exclusively in a (4,0) isomeric form while a mixture of (4,0) and (3,1) isomers is obtained from synthesis of the Rh_2^{5+} derivatives with 2,6-F_2ap, 2,4,6-F_3ap, or F_5ap bridging ligands.

Molecular Structures. Selected average bond lengths and average bond angles of (4,0) Rh_2(2-Fap)$_4$Cl (**1**), (4,0) Rh_2(2,6-F_2ap)$_4$Cl (**2**), (3,1) Rh_2(2,6-F_2ap)$_4$Cl (**3**), and (3,1) Rh_2(F_5ap)$_4$Cl (**7**) are summarized in Table 3 while Figures 1 and 2 illustrate ORTEP diagrams of compounds **1**−**3** and **7**. Selected average bond lengths and average bond angles

Table 3. Selected Average Bond Lengths and Bond Angles of the (4,0) Isomers of Rh_2(L)$_4$Cl, Where L = ap, 2-Fap (**1**), or 2,6-F_2ap (**2**)

ligand, L	ap	2-Fap (**1**)	2,6-F_2ap (**2**)
	Bond Lengths (Å)		
Rh−Rh	2.406	2.412	2.416
Rh−Cl	2.421	2.431	2.465
Rh−N_a[a]	2.008	2.007	2.023
Rh−N_p[b]	2.048	2.063	2.057
	Bond Angles (deg)		
Rh−Rh−Cl	180.00	180.00	180.00
Rh−Rh−N_a	87.00	87.30	86.74
Rh−Rh−N_p	86.60	86.60	86.45
N_a−Rh−Rh−N_p	23.40	21.39	24.32

[a] N_a: anilino nitrogen. [b] N_p: pyridyl nitrogen.

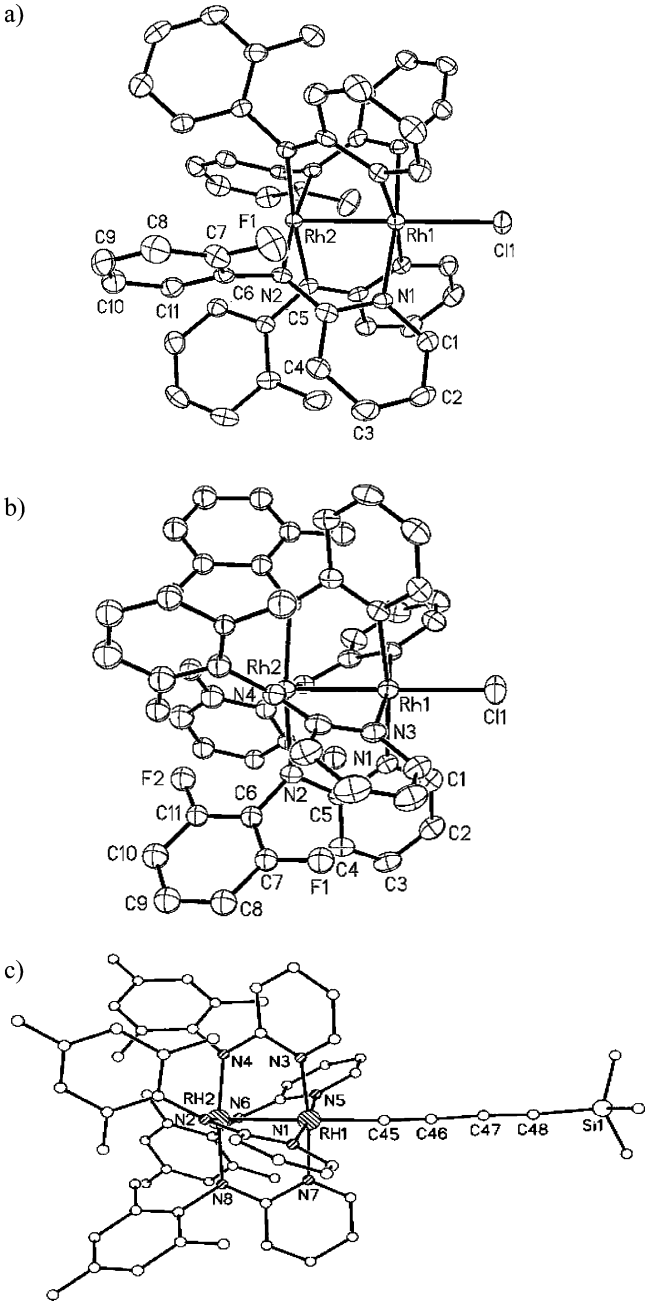

Figure 1. Molecular structure of the (4,0) isomers of (a) $Rh_2(2\text{-Fap})_4Cl$ (**1**), (b) $Rh_2(2,6\text{-}F_2ap)_4Cl$ (**2**), and (c) $Rh_2(2,4,6\text{-}F_3ap)_4(C{\equiv}C)_2Si(CH_3)_3$ (**9**). H atoms have been omitted for clarity.

of (3,1) $Rh_2(2,6\text{-}F_2ap)_4CN$ (**8**) are summarized in Table 4. Figure 2c illustrates the ORTEP diagram of this compound while Figure 1c shows the structure of (4,0) $Rh_2(2,4,6\text{-}F_3ap)_4(C{\equiv}C)_2Si(CH_3)_3$ for the purpose of geometric isomer identification. All intramolecular bond lengths and bond angles as well as other structural data of these compounds are given in the Supporting Information.

The coordination of Rh1 and Rh2 in compounds **1**−**3** and **7**−**9** is essentially octahedral and square pyramidal, respectively, with four "substituted ap" bridging ligands forming the equatorial plane. In the case of the (4,0) isomers, Rh1 is coordinated to the chloride axial ligand for **1** and **2** or to the $(C{\equiv}C)_2Si(CH_3)_3$ ligand for **9** and to four pyridyl nitrogens while Rh2 is coordinated to four anilino nitrogens. For the

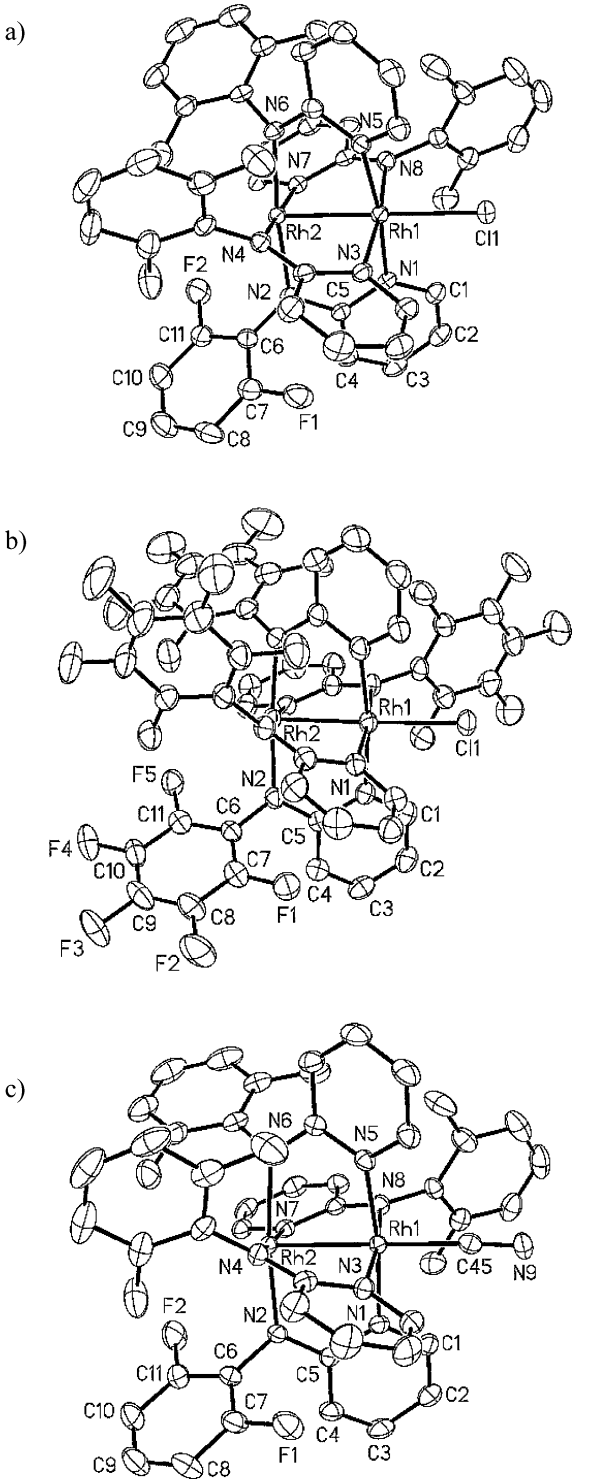

Figure 2. Molecular structure of the (3,1) isomers of (a) $Rh_2(2,6\text{-}F_2ap)_4Cl$ (**3**), (b) $Rh_2(F_5ap)_4Cl$ (**7**), and (c) $Rh_2(2,6\text{-}F_3ap)_4CN$ (**8**). H atoms have been omitted for clarity.

(3,1) isomers, Rh1 is coordinated to the axial chloride ligand for **3** and **7** or to the cyanide ligand for **8** as well as to three pyridyl nitrogens and one anilino nitrogen while Rh2 is coordinated to three anilino nitrogens and one pyridyl nitrogen.

As discussed below and shown in Table 3 for the case of $Rh_2(L)_4Cl$ where L = 2-Fap, 2,6-F_2ap, or F_5ap, there is no specific effect of the dimetal core on the structural properties

Table 4. Selected Average Bond Lengths and Bond Angles of the (3,1) Isomers of $Rh_2(F_5ap)_4Cl$ (**7**) and $Rh_2(2,6\text{-}F_2ap)_4L_{ax}$, Where $L_{ax} = Cl^-$ (**3**) or CN^- (**8**)

ligand, L	F_5ap (**7**)	2,6-F_2ap (**3**)	2,6-F_2ap (**8**)
	Bond Lengths (Å)		
Rh−Rh	2.415	2.420	2.447
Rh−L_{ax}	2.438	2.417	2.031
Rh−N_a[a]	2.020	2.020	2.027
Rh−N_p[b]	2.054	2.055	2.063
	Bond Angles (deg)		
Rh−Rh−L_{ax}	177.93	178.80	179.12
Rh−Rh−N_a	87.40	87.13	86.97
Rh−Rh−N_p	86.60	86.87	86.85
N_a−Rh−Rh−N_p	20.76	20.53	20.16

[a] N_a: anilino nitrogen. [b] N_p: pyridyl nitrogen.

Table 5. Yields (and Isomeric Distribution) of $Rh_2(L)_4Cl$ Complexes, Where L = ap, 2-Fap, 2,6-F_2ap, 2,4,6-F_3ap, or F_5ap

ligand, L	(4,0) isomer	(3,1) isomer
ap	60%[a]	not formed
2-Fap	60% **(1)**	not formed
2,6-F_2ap	25% **(2)**	30% **(3)**
2,4,6-F_3ap	18% **(4)**	27% **(5)**
F_5ap	10% **(6)**	20% **(7)**

[a] Taken from ref 4.

of the compounds and the same trends observed among the (4,0) or (3,1) isomer of $Rh_2(L)_4Cl$ are also seen for the (4,0) and (3,1) isomers of $Ru_2(L)_4Cl$.[11] For example, the isomer effect on the M−M and M−Cl bond lengths as well as that on the $M_2(L)_4$ framework, M−M−Cl bond angles, and N−M−M−N torsion angles are virtually the same for M = Ru or Rh. More specifically, the Rh−Rh bond lengths of **1**−**3** and **7** range from 2.412 to 2.420 Å and there is no significant isomer effect on the metal−metal bond. As shown in Table 3, the $Rh_2(L)_4$ framework is not significantly affected by the type of briding ligand and/or the isomeric form of the complex.

Structural studies of $Ru_2(L)_4Cl$[11] where L is an ap-substituted ligand revealed different trends of the M−M−Cl bond angles in the (4,0) and (3,1) isomer series, and, as shown in Table 3, this is also the case for the (4,0) and (3,1) isomers of $Rh_2(L)_4Cl$. For instance, all three (4,0) isomers are characterized by a Rh−Rh−Cl bond angle of 180.0° but the Rh−Rh−Cl bond angles of the (3,1) isomers decrease from 178.8° to 177.93°. There is also no effect of the dimetal core on the torsion angles of the (4,0) and (3,1) isomers because the (4,0) isomers exhibit larger N−M−M−N torsion angles than the (3,1) isomers in both the Ru_2 and Rh_2 series of complexes.

As shown in Table 4, no significant structural difference is observed in the 2,6-F_2ap framework upon going from (3,1) $Rh_2(2,6\text{-}F_2ap)_4CN$ (**8**) to its parent complex, (3,1) $Rh_2(2,6\text{-}F_2ap)_4Cl$ (**3**), but the Rh−Rh bond length increases from 2.420 Å (chloro derivative) to 2.447 Å (cyano derivative) owing to differences in the donor ability of the axial ligands.

The isomeric distribution and yields of each $Rh_2(L)_4Cl$ isomer (L is one of the four bridging ligands shown in Chart 1) are given in Table 5. The compound with a singly substituted ap ligand, $Rh_2(2\text{-}Fap)_4Cl$, exists exclusively as the (4,0) isomer while the three others with 2, 3, or 5 F groups per ap, $Rh_2(2,6\text{-}F_2ap)_4Cl$, $Rh_2(2,4,6\text{-}F_3ap)_4Cl$, and $Rh_2(F_5ap)_4Cl$, form both the (4,0) and (3,1) isomers with the (3,1) isomer being preferred. The yields of the (4,0) and (3,1) isomers also vary with the type of bridging ligand (see Table 5). The compounds which possess F groups at both ortho positions of the phenyl rings of the ap-type ligand, $Rh_2(2,6\text{-}F_2ap)_4Cl$, $Rh_2(2,4,6\text{-}F_3ap)_4Cl$, and $Rh_2(F_5ap)_4Cl$ (see Chart 1), are the only ones to exist in more than one isomeric form. This result parallels what was reported for the related Ru_2(III,II) complexes,[11] thus suggesting no significant effect of the dimetal core, i.e., Ru_2 or Rh_2, on the isomeric distribution. However, it should be pointed out that $Rh_2(2\text{-}Fap)_4Cl$ and $Ru_2(2\text{-}Fap)_4Cl$[9] exist in two different isomeric forms; the Rh_2^{5+} species is only formed as a (4,0) isomer while only the (3,1) isomer is seen in the case of the Ru_2^{5+} species.

ESR Studies. The ESR spectra of compounds **1**−**7** in degassed CH_2Cl_2/CH_3CN at 77 K are similar to each other (see Table 6 and Figures S1 and S2, Supporting Information), and all have features identical to the spectrum reported for $Rh_2(ap)_4Cl$.[3,4] They are typical of compounds with axial symmetry and exhibit two signals in the range of $g_\perp$ = 2.058−2.069 and $g_{||}$ = 1.913−1.939. The $g_{||}$ component is split into a doublet with $A_{||}$ in the range of 20.0−25.0 × 10^{-4} cm^{-1} (see Table 6). The odd electron of $Rh_2(ap)_4Cl$, $Rh_2(ap)_4(C{\equiv}CH)$, and $Rh_2(ap)_4(C{\equiv}C)_2Si(CH_3)_3$ has been shown to be localized on only one of the two rhodium atoms,[3,5,10] and a similar assignment is proposed for the odd electron of compounds **1**−**7** on the basis of their ESR spectra.

The $g_{||}$ values for all the compounds in Table 6 are less than g_e, thus indicating that the SOMO is a δ^*_{Rh-Rh} orbital. A similar assignment was earlier made for $Rh_2(ap)_4Cl$, $Rh_2(ap)_4(C{\equiv}CH)$ and $Rh_2(ap)_4(C{\equiv}C)_2Si(CH_3)_3$.[3,5,10] Although there is no significant difference in g values among compounds **1**−**7**, the $A_{||}$ values systematically decrease upon going from L = Fap to F_5ap, thus implying that the polarization of the SOMO is strongly affected by the donor ability of the bridging ligand. The magnitude of $A_{||}$ is related to the spin density at the nucleus or nuclei;[35] the higher the spin density at the nuclei, the larger is the value of $A_{||}$.

The SOMO is known to be δ^*_{Rh-Rh}, when $g_{||} < g_e$ and both theoretical and experimental studies of **g** tensors for Rh_2^{5+} complexes predict $g_{||} < g_\perp$ when the SOMO is δ^*_{Rh-Rh} and $g_{||} > g_\perp$ when it is σ^*_{Rh-Rh} or π^*_{Rh-Rh}.[3,36−38] Therefore the **g** tensors for compounds **1**−**7** are consistent with δ^*_{Rh-Rh} as the SOMO. Hence, one can propose that the SOMO is δ^*_{Rh-Rh}, independent of the isomer type or the basicity of the bridging ligand. We also propose that the effect of the bridging ligand on the $A_{||}$ can be accounted for by changes in the electronic field of the Rh_2^{5+} core due to a difference in the bridging ligand basicity as discussed in the next paragraph.

(35) Wertz, J. E.; Bolton, J. R. *Electron Spin Elementary Theory and Practical Applications*; Chapman and Hall: New York, 1986.
(36) Lindsay, A. J.; Wilkinson, G.; Motevalli, M.; Hursthouse, M. B. *J. Chem. Soc., Dalton Trans.* **1985**, 2321.
(37) Cotton, F. A.; Feng, X. *Inorg. Chem.* **1989**, *28*, 1180.
(38) Cotton, F. A.; Matusz, M. *J. Am. Chem. Soc.* **1988**, *110*, 5761.

Table 6. ESR Data (in CH_2Cl_2/CH_3CN under Ar at 77 K) and Room Temperature Effective Magnetic Moment (μ, μ_B) of $Rh_2(L)_4Cl$ Complexes

		(4,0) isomer				(3,1) isomer			
			ESR				ESR		
ligand $\sum\sigma$	ligand L	compd no.	$g_\perp$	$g_\parallel$ (10^4 $A_\parallel$, cm^{-1})	μ (μ_M)	compd no.	$g_\perp$	$g_\parallel$ (10^4 $A_\parallel$, cm^{-1})	μ (μ_M)
0.00	ap[a]		2.090	1.950 (27.0)	1.88				
0.24	2-Fap	**1**	2.058	1.939 (25.0)	2.00				
0.48	2,6-F_2ap	**2**	2.058	1.936 (23.8)	1.91	**3**	2.069	1.913 (23.1)	1.98
0.54	2,4,6-F_3ap	**4**	2.058	1.937 (23.4)	1.78	**5**	2.059	1.934 (22.8)	1.87
1.22	F_5ap	**6**	2.058	1.928 (20.0)	1.93	**7**	2.065	1.921 (20.5)	1.92

[a] Taken from ref 4.

Table 7. Half-Wave Potentials (V vs SCE) for Redox Processes of the (4,0) and (3,1) Isomers of $Rh_2(L)_4Cl$ in CH_2Cl_2 Containing 0.1 M TBAP

isomer type	ligand, $\sum\sigma$	ligand, L	oxidation		reduction	$\Delta E_{1/2}$[a] (V)
			Rh_2^{7+}/Rh_2^{6+}	Rh_2^{6+}/Rh_2^{5+}	Rh_2^{5+}/Rh_2^{4+}	
(4,0)	0.00	ap		0.52	−0.38	0.90
	0.24	2-Fap (**1**)		0.64	−0.25	0.89
	0.48	2,6-F_2ap (**2**)	1.49	0.78	−0.14	0.92
	0.54	2,4,6-F_3ap (**4**)	1.54	0.85	−0.07	0.92
	1.22	F_5ap (**6**)		1.09	0.20	0.89
(3,1)	0.48	2,6-F_2ap (**3**)	1.53	0.75	−0.13	0.88
	0.54	2,4,6-F_3ap (**5**)	1.54	0.81	−0.07	0.88
	1.22	F_5ap (**7**)		0.98	0.18	0.80

[a] |1st ox. − 1st red.|.

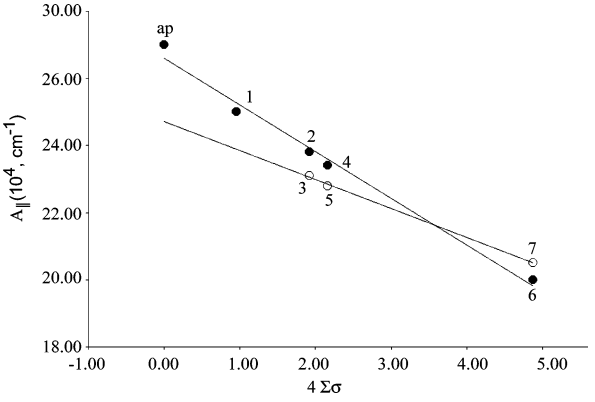

Figure 3. Correlation between the $A_\parallel$ and $4\sum\sigma$ for the (4,0) isomer (●) and (3,1) isomer (○) of $Rh_2(L)_4Cl$ (L = ap, 2-Fap, 2,6-F_2ap, 2,4,6-F_3ap, or F_5ap). Values of $A_\parallel$ and $\sum\sigma$ are given in Table 6.

Plots of the $A_\parallel$ values of compounds **1**−**7** vs the sum of the substituent constants ($\sum\sigma$) of the bridging ligand[39] are shown in Figure 3 and display a linear relationship for both the (4,0) and (3,1) isomers. In both types of isomers, the $A_\parallel$ values decrease with increase in the overall electron-withdrawing effect of the bridging ligands, consistent with the fact that the electronegative F atoms lead to a decrease in spin density at the dirhodium unit.

The room-temperature magnetic moments of compounds **1**−**7** are given in Table 6 and fall in the range of 1.78−2.00 μ_B, thus suggesting that each compound contains a single unpaired electron. $Rh_2(ap)_4Cl$, $Rh_2(ap)_4(C{\equiv}CH)$ and $Rh_2(ap)_4(C{\equiv}C)_2Si(CH_3)_3$ have been assigned[3,5,10] the electronic configuration $\sigma^2\pi^4\delta^2\pi^{*4}\delta^{*1}$ and, on the basis of the ESR and magnetic data, this electronic configuration can also be proposed for compounds **1**−**7**.

Compound **8** and its parent complex, (3,1) Rh_2(2,6-F_2ap)$_4$Cl (**3**), have similar ESR features, and similar properties are also seen for compound **9** and its parent complex, (4,0) Rh_2(2,4,6-F_3ap)$_4$Cl (**4**), which suggests a very similar electron density distribution in both sets of compounds of each isomer type.

The g and $A_\parallel$ values of (3,1) Rh_2(2,6-F_2ap)$_4L_{ax}$ (L_{ax} = axial ligand) and (4,0) Rh_2(2,4,6-F_3ap)$_4L_{ax}$ systematically increase upon switching the axial ligand from Cl^- to CN^- in the case of the (3,1) isomer and from Cl^- to $(C{\equiv}C)_2Si(CH_3)_3^-$ in the case of the (4,0) isomer (see Table S1, Supporting Information), thus suggesting that the SOMO is clearly affected by the donor ability of the axial ligands, independent of the isomer type. However, the SOMO of **8** and **9** is still assigned as δ^*_{Rh-Rh} and variations in the ESR parameters can then simply be accounted for by an effect of axial donor strength on the g and $A_\parallel$ values owing to changes in the electronic field of the Rh_2^{5+} core upon going from Cl^- to CN^- or $(C{\equiv}C)_2Si(CH_3)_3^-$. There is no evidence for a switch in the electronic configuration of the compounds upon going from Rh_2(2,6-F_2ap)$_4$Cl (**3**) to Rh_2(2,6-F_2ap)$_4$CN (**8**) or Rh_2(2,4,6-F_3ap)$_4$Cl (**4**) to Rh_2(2,4,6-F_3ap)$_4(C{\equiv}C)_2Si(CH_3)_3$ (**9**), and the electronic configuration $\sigma^2\pi^4\delta^2\pi^{*4}\delta^{*1}$ is therefore proposed for all of the investigated compounds in this study.

Electrochemistry. The redox behavior of compounds **1**−**7** was investigated by cyclic voltammetry in CH_2Cl_2 containing 0.1 M TBAP, and half-wave potentials for each electrode reaction of the investigated compounds are listed in Table 7 along with data of $Rh_2(ap)_4Cl$ for comparison purposes.

Cyclic voltammograms of **1**, **2**, **4**, and **6** are shown in Figure 4 while cyclic voltammograms of **3**, **5**, and **7** are illustrated in Figure 5. Two different types of behavior are observed among the Rh_2 complexes. One is given by the ap complex as well as compounds **1**, **6**, and **7** which undergo one reversible one-electron reduction and one reversible one-electron oxidation. This contrasts with what is seen for complexes **2**−**5**, which undergo one reversible one-electron

(39) Zuman, P. *Substituent Effects in Organic Polarography*; Plenum Press: New York, 1967.

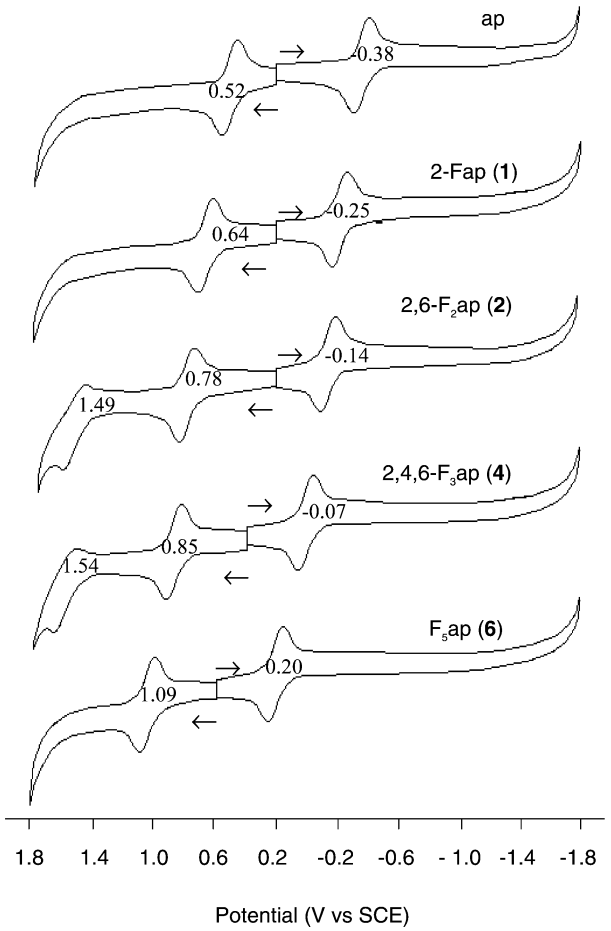

Figure 4. Cyclic voltammograms of (4,0) $Rh_2(L)_4Cl$ (L = 2-Fap, 2,6-F_2ap, 2,4,6-F_3ap, or F_5ap) in CH_2Cl_2 containing 0.1 M TBAP. Scan rate = 0.1 V/s.

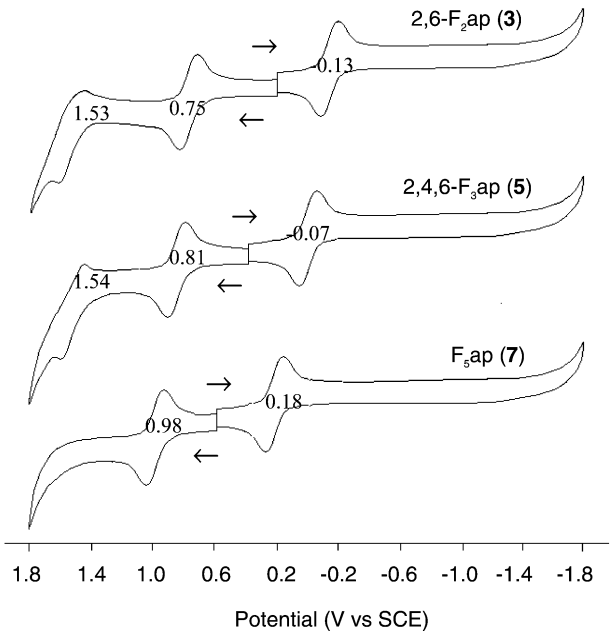

Figure 5. Cyclic voltammograms of (3,1) $Rh_2(L)_4Cl$ (L = 2,6-F_2ap, 2,4,6-F_3ap, or F_5ap) in CH_2Cl_2 containing 0.1 M TBAP. Scan rate = 0.1 V/s.

reduction but two reversible one-electron oxidations. Most conspicuous by its absence is the second oxidation of $Rh_2(ap)_4Cl$ and $Rh_2(2\text{-Fap})_4Cl$ which would be expected to

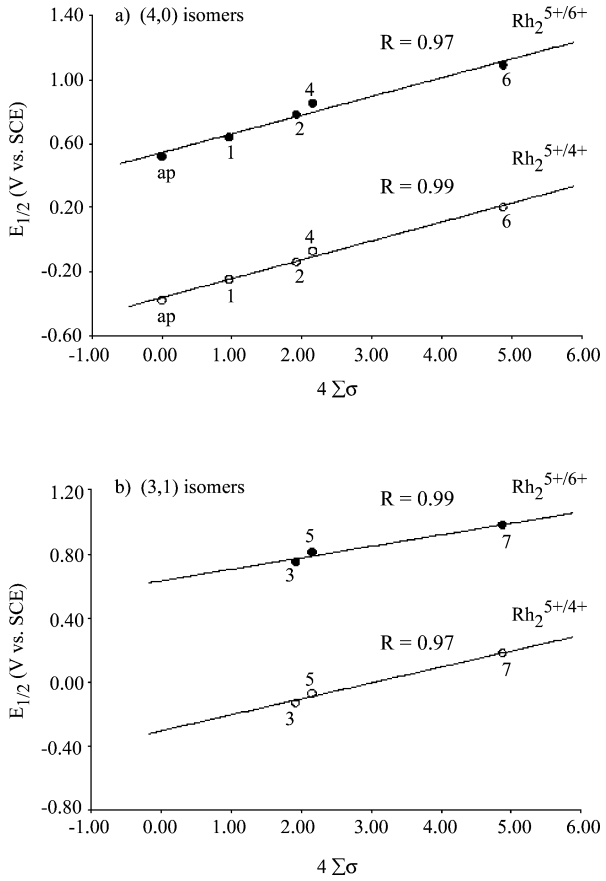

Figure 6. Linear free energy relationships between $E_{1/2}$ and $4\sum\sigma$ for the oxidation (●) and reduction (○) of (a) (4,0) and (b) (3,1) isomeric complexes of $Rh_2(L)_4Cl$.

occur at $E_{1/2}$ values between 1.25 and 1.35 V and is clearly "missing" from these compounds. We cannot comment on the two F_5ap complexes since this electrode reaction may be located at $E_{1/2}$ values beyond the potential range of the solvent.

Plots of $E_{1/2}$ vs the sum of substituent constants ($\sum\sigma$)[39] for the reduction and first oxidation of (4,0) $Rh_2(L)_4Cl$ (L = ap, 2-Fap, 2,6-F_2ap, 2,4,6-F_3ap, or F_5ap) are shown in Figure 6a while similar plots for (3,1) $Rh_2(L)_4Cl$ (L = 2,6-F_2ap, 2,4,6-F_3ap, or F_5ap) are shown in Figure 6b. The dependence of $E_{1/2}$ on the electronic effect of the substituents can be quantified by a linear least-squares fit of the data using the Hammett relationships shown in eq 3:[40,41]

$$\Delta E_{1/2} = E_{1/2}(X) - E_{1/2}(H) = 4\sum\sigma\rho \qquad (3)$$

where ρ is the reactivity constant. Since there are four equivalent bridging ligands on each investigated dirhodium complex, $4\sum\sigma$ is used in eq 3. The R values of the two lines in Figure 6 range from 0.97 to 0.99, thus clearly suggesting that there is no change in electron-transfer mechanism for compounds in either the (4,0) or (3,1) isomer series. Hence, all redox processes of each Rh_2^{5+} species involve the dimetal unit and the reduction is described by eq 4 while the first

(40) Zuman, P. *The Elucidation of Organic Electrode Process*; Academic Press: London, 1967.
(41) Hammett, L. P. *Physical Organic Chemistry*; Wiley: New York, 1970.

and second oxidations are given by eqs 5 and 6, respectively.

$$(L)_4Rh_2^{5+} + e^- \rightleftarrows (L)_4Rh_2^{4+} \quad (4)$$

$$(L)_4Rh_2^{5+} \rightleftarrows (L)_4Rh_2^{6+} + e^- \quad (5)$$

$$(L)_4Rh_2^{6+} \rightleftarrows (L)_4Rh_2^{7+} + e^- \quad (\mathbf{2}-\mathbf{5}\ \text{only}) \quad (6)$$

As shown in Table 7, the type of geometric isomer, i.e., (4,0) or (3,1), has no significant effect on the $E_{1/2}$ of a given electrode reaction of $Rh_2(L)_4Cl$, and consequently very similar values of $\Delta E_{1/2}$ are seen for the (3,1) and (4,0) isomers. For instance, $E_{1/2}$ for the first oxidation of $Rh_2(2,6\text{-}F_2ap)_4Cl$, i.e., the $Rh_2^{5+/6+}$ process, is shifted cathodically by only 30 mV upon going from the (3,1) to the (4,0) isomer and the reductions of both isomers have the same $E_{1/2}$ values within experimental error (±10 mV). A similar trend is also observed for oxidation and reduction of $Rh_2(2,4,6\text{-}F_3ap)_4Cl$ and $Rh_2(F_5ap)_4Cl$, but there is a more significant difference in $E_{1/2}$ between the oxidations of the (4,0) isomer (1.09 V) and the (3,1) isomer (0.98 V) of $Rh_2(F_5ap)_4Cl$; this is most likely because the electronic perturbation upon going from the (4,0) to the (3,1) isomer increases in the order: $F_2ap < F_3ap < F_5ap$. A similar isomer effect on the redox potentials was also reported for Ru_2^{5+} complexes with the same type of bridging ligands,[11] but in this case the $Ru_2^{5+/6+}$ process was more sensitive to the isomer type.

Redox potentials for the three electrode reactions of (3,1) $Rh_2(2,6\text{-}F_2ap)_4CN$ (**8**) are located at −0.23, 0.75, and 1.53 V vs SCE (see Table S1) while the parent complex, (3,1) $Rh_2(2,6\text{-}F_2ap)_4Cl$ (**3**), is reduced at −0.13 V and oxidized at 0.75 and 1.53 V (see Table 7). There is thus no effect of the axial ligand on the two oxidations. We previously reported that the addition of (TBA)Cl or (TBA)CN to solutions of $Rh_2(ap)_4Cl$ has no effect on any of the redox potentials, even at high concentrations of added anion,[4] and this is also the case for $Rh_2(2,6\text{-}F_2ap)_4Cl$.

The coordination of Cl^- or CN^- to (3,1) $Rh_2(2,6\text{-}F_2ap)_4Cl$ (**3**) or $Rh_2(2,6\text{-}F_2ap)_4CN$ (**8**) was monitored by cyclic voltammetry in the presence of excess anion to see if a bis-adduct might be generated. Dichloromethane solutions containing increased amounts of (TBA)Cl or (TBA)CN were added to a CH_2Cl_2, 0.1 M TBAP solution of **3**, and cyclic voltammograms were recorded after each addition. The addition of up to 1000 equiv of (TBA)Cl to compound **3** has no effect on the redox potentials, thus implying that no bis-Cl^- adduct is formed in solution. However, upon addition of 1 equiv of (TBA)CN to **3**, a new wave at $E_{1/2} = -0.23$ V begins to appear and the wave at $E_{1/2} = -0.13$ V decreases in intensity. At the same time, the two oxidation processes remain unchanged. The addition of more (TBA)CN has no further effect on the redox potentials, and the $E_{1/2}$ values obtained in the presence of up to 1000 equiv of CN^- are identical to the $E_{1/2}$ values obtained for (3,1) $Rh_2(2,6\text{-}F_2ap)_4CN$, thus suggesting a simple CN^- for Cl^- anion exchange in solution. The addition of (TBA)Cl or (TBA)CN to compound **8** also has no effect on the redox potentials, even at high concentrations of added salt, thus implying that CN^- dissociates very slowly from (3,1) $Rh_2(2,6\text{-}F_2ap)_4CN$ and that a bis-CN^- adduct of Rh_2^{5+} or Rh_2^{4+} is not formed in solution.

The three electrode reactions of (4,0) $Rh_2(2,4,6\text{-}F_3ap)_4(C{\equiv}C)_2Si(CH_3)_3$ (**9**) are located at $E_{1/2} = -0.27$, 0.75 and 1.40 V vs SCE (see Table S1) while its parent complex, (4,0) $Rh_2(2,4,6\text{-}F_3ap)_4Cl$ (**4**), is reduced at $E_{1/2}$ = -0.07 V and oxidized at $E_{1/2} = 0.85$ and 1.54 V (see Table 7). Thus, the reduction half-wave potential is negatively shifted by 200 mV upon changing the axial ligand from Cl^- to $(C{\equiv}C)_2Si(CH_3)_3^-$ in the case of (4,0) $Rh_2(2,4,6\text{-}F_3ap)_4L_{ax}$ and a 100 mV shift in potential is observed upon going from (3,1) $Rh_2(2,6\text{-}F_2ap)_4Cl$ (**3**) to $Rh_2(2,6\text{-}F_2ap)_4CN$ (**8**). Smaller differences in $E_{1/2}$ are seen for the first oxidation of the same compounds where the half-wave potentials are negatively shifted by 100 mV upon going from compound **4** to compound **9**, and there is no change upon going from compound **3** to compound **8** where $E_{1/2}$ values for oxidation are identical under the same experimental conditions.

UV−Vis Spectra. The UV−vis absorption features of the investigated compounds in their Rh_2^{4+}, Rh_2^{5+}, and Rh_2^{6+} forms are summarized in Table 8. All Rh_2^{5+} complexes exhibit four absorption bands (labeled as I−IV in Table 8), except for the ap and 2-Fap derivatives, which show only three bands, I, II, and IV. The λ_{max} of band IV for Rh_2^{5+} in the (4,0) isomer series of compounds varies from 910 to 1009 nm and appears to be the most sensitive to the type of bridging ligand. Band IV of Rh_2^{5+} in the (3,1) isomer series also shows the same type of behavior, but no isomers of this type were formed for ap or Fap to confirm this result.

The $Rh_2(ap)_4ClO_4$ complex is known to display a low energy, intense $\pi(N) \rightarrow \delta^*(Rh_2)$ LMCT band at 890 nm ($\epsilon = 3.330 \times 10^3\ M^{-1}\ cm^{-1}$),[42,43] and band IV of $Rh_2(ap)_4Cl$ and the other Rh_2^{5+} complexes in Table 8 is proposed to originate from the same electronic transition. The present data are, however, insufficient to assign any electronic transition to the other three bands.

The UV−visible spectrum of $Rh_2(L)_4Cl$ (L = 2,6-F_2ap, 2,4,6-F_3ap, or F_5ap) also appears to be sensitive to the isomer type (see Table 8). For example, the (4,0) and (3,1) isomers of $Rh_2(2,6\text{-}F_2ap)_4Cl$ both exhibit four absorption bands (see Figure 7); the molar absorptivities of the lowest and highest energy transitions are similar in the case of the (4,0) isomer log $\epsilon = 3.4$ and 3.8 but not in the case of the (3,1) isomer where ϵ varies by two log units (see Table 8). In addition, band III of each (3,1) isomer is systematically blue-shifted and has a higher molar absorptivity than band III of the corresponding (4,0) isomer. Hence, one should be able to differentiate the (4,0) isomer from the (3,1) isomer of these compounds on the basis of the UV−visible spectra, and this argument is used in the present paper to assign a proposed isomer type for (3,1) $Rh_2(2,4,6\text{-}F_3ap)_4Cl$ and (4,0) $Rh_2(F_5ap)_4$-

(42) Yao, C. L.; Park, K. H.; Khokhar, A. R.; Jun, M. J.; Bear, J. L. *Inorg. Chem.* **1990**, *29*, 4033.

(43) Miskowski, V. M.; Hopkins, M. D.; Winkler, J. R.; Gray, H. B. Multiple Metal-Metal Bonds. In *Inorganic Electronic Structure And Spectroscopy*; Solomon, E. I., Lever, A. B. P., Eds.; John Wiley & Sons: New York, 1999; Vol. 2.

Table 8. UV−Vis Spectral Data of (4,0) and (3,1) $Rh_2(L)_4Cl$ (L = ap, 2-Fap, 2,6-F_2ap, 2,4,6-F_3ap, or F_5ap) in CH_2Cl_2 Containing 0.2 M TBAP

isomer type	oxidation state	ligand	λ_{max}, nm ($\epsilon \times 10^{-3}$, M^{-1} cm^{-1}) band I	band II	band III	band IV
(4,0)	Rh_2^{6+}	ap	492 (5.5)	567 (5.6)		903 (3.0)
		2-Fap (**1**)	497 (5.4)	581 (5.6)		930 (3.3)
		2,6-F_2ap (**2**)	510 (5.7)	574 (5.7)		970 (2.8)
		2,4,6-F_3ap (**4**)	515 (5.6)	577 (5.6)		971 (3.0)
		F_5ap (**6**)	545 (6.2)			1000 (3.8)
	Rh_2^{5+}	ap	495 (3.2)	572 (sh)		910 (5.1)
		2-Fap (**1**)	497 (3.5)	559 (2.6)		920 (5.1)
		2,6-F_2ap (**2**)	505 (3.4)	561 (sh)	718 (0.5)	977 (3.8)
		2,4,6-F_3ap (**4**)	500 (3.7)	561 (sh)	711 (0.6)	990 (3.8)
		F_5ap (**6**)	535 (sh)	542 (2.3)	700 (0.6)	1009 (3.7)
	Rh_2^{4+}	ap	501 (2.7)	642 (0.4)		
		2-Fap (**1**)	485 (2.8)	630 (0.5)		
		2,6-F_2ap (**2**)	480 (2.8)	642 (0.5)		
		2,4,6-F_3ap (**4**)	481 (2.9)	630 (0.4)		
		F_5ap (**6**)	478 (2.3)			
(3,1)	Rh_2^{6+}	2,6-F_2ap (**3**)	525 (5.0)	597 (sh)		987 (3.8)
		2,4,6-F_3ap (**5**)	516 (5.9)	575 (sh)		990 (3.2)
		F_5ap (**7**)	550 (6.4)			1012 (3.7)
	Rh_2^{5+}	2,6-F_2ap (**3**)	517 (2.8)	542 (2.8)	695 (1.2)	1004 (5.0)
		2,4,6-F_3ap (**5**)	512 (2.9)	542 (2.9)	692 (0.9)	1000 (5.4)
		F_5ap (**7**)	549 (2.7)	580 (2.9)	688 (0.9)	1029 (4.4)
	Rh_2^{4+}	2,6-F_2ap (**3**)	480 (2.4)	635 (0.8)		
		2,4,6-F_3ap (**5**)	470 (2.6)	623 (0.7)		
		F_5ap (**7**)	485 (2.5)			

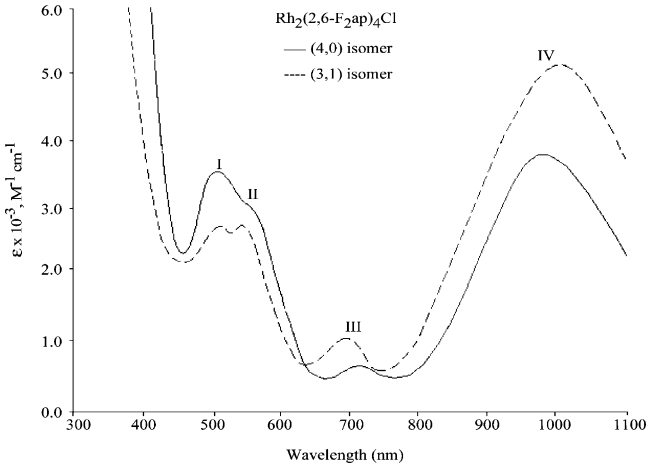

Figure 7. UV−visible spectra of the (4,0) isomer (—) and (3,1) isomer (- - -) of $Rh_2(2,6\text{-}F_2ap)_4Cl$ in CH_2Cl_2.

Cl whose structures could not be confirmed by single-crystal X-ray diffraction.

The singly reduced and singly oxidized forms of the (4,0) and (3,1) isomers of $Rh_2(L)_4Cl$ (L = ap, 2-Fap, 2,6-F_2ap, 2,4,6-F_3ap, or F_5ap) were in-situ generated in a thin-layer spectroelectrochemical cell, and examples of UV−visible spectral changes which occur during the $Rh_2^{5+/4+}$ and $Rh_2^{5+/6+}$ electrode processes of the (4,0) and (3,1) isomers of $Rh_2(2,6\text{-}F_2ap)_4Cl$ are shown in Figures 8 and 9, respectively.

Six of the electrogenerated Rh_2^{6+} complexes in Table 8 display three absorption bands while both isomers of $Rh_2(F_5ap)_4Cl$ (**6** and **7**) lack a band II. Overall, spectral features of the Rh_2^{6+} derivatives in Table 8 are similar to what has been reported for $[Rh_2(ap)_4(C{\equiv}CH)]^+$ (λ_{max} = 450, 580, and 910 nm), a compound whose electronic structure has been

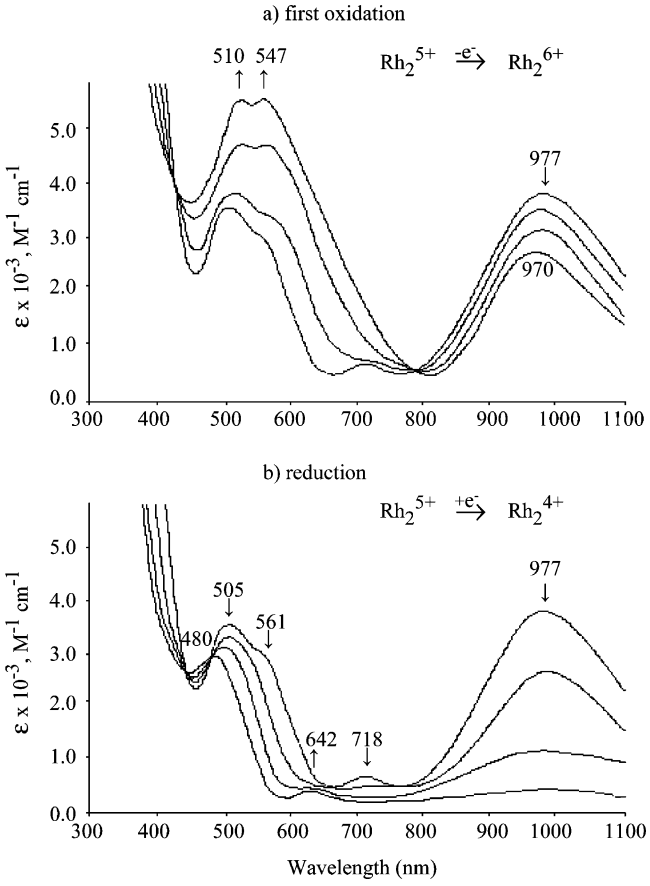

Figure 8. Time-dependent UV−visible thin-layer spectral changes during of (a) first oxidation and (b) first reduction of (4,0) $Rh_2(2,6\text{-}F_2ap)_4Cl$ (**2**) in CH_2Cl_2 containing 0.2 M TBAP under Ar.

proposed[5] as $\sigma^2\pi^4\delta^2\pi^*$.[4] This orbital assignment implies that an electron is removed from the δ^* orbital upon going from

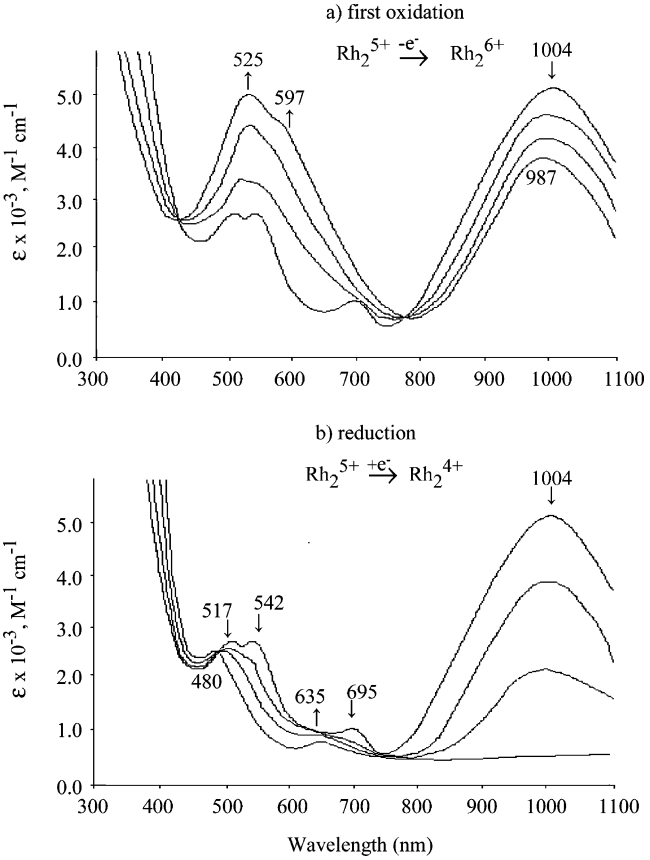

Figure 9. Time-dependent UV−visible thin-layer spectral changes during (a) first oxidation and (b) reduction of (3,1) $Rh_2(2,6\text{-}F_2ap)_4Cl$ (**3**) in CH_2Cl_2, 0.2 M TBAP under Ar.

the Rh_2^{5+} to the Rh_2^{6+} form of each compound in Table 8. The data also suggests that the same electron-transfer mechanism occurs upon oxidation of each compound; this agrees with the observed linear free energy relationship between $E_{1/2}$ and $4\sum\sigma$ (Figure 6).

Most of the Rh_2^{4+} derivatives in Table 8 exhibit similar UV−visible features, and in each case the spectrum lacks both a band III and a band IV. We have assigned band IV as a $\pi(N) \rightarrow \delta^*(Rh_2)$ transition; the fact that this band vanishes upon reduction suggests that the electron is added to a δ^* orbital, consistent with an electronic configuration of $\sigma^2\pi^4\delta^2\pi^{*4}\delta^{*2}$ for the Rh_2^{4+} forms of each compound in Table 8.

The λ_{max} of the higher energy visible bands of the Rh_2(III, II) complexes are known to be influenced by the σ donor ability of the axial anion,[5] and this is also what is seen for (3,1) $Rh_2(2,6\text{-}F_2ap)_4L_{ax}$ upon switching the axial ligand from $L_{ax} = Cl^-$ to $L_{ax} = CN^-$. For example, the λ_{max} of bands I, II, and III are located at 517, 542, and 695 nm, respectively, for the chloro complex but appear at 433, 478, and 648 nm for the cyano derivative. In addition, it should be noted that band IV blue shifts from 1004 to 862 nm upon going from Cl^- to CN^-. The UV−visible bands of (4,0) $Rh_2(2,4,6\text{-}F_3ap)_4(C{\equiv}C)_2Si(CH_3)_3$ (**9**) are located at 460, 547, and 878 nm (see Table S1) while its parent complex, (4,0) $Rh_2(2,4,6\text{-}F_3ap)_4Cl$ (**4**), has absorption bands at 500, 561, 711, and 990 nm (see Table 8). A similar difference in λ_{max} has been reported for (4,0) $Rh_2(ap)_4L_{ax}$ where $L_{ax} = Cl^-$ or $C{\equiv}CR^-$, thus suggesting that the absorption peak maxima of the UV−visible bands are a function of the type of axial ligand bound to the dimetal unit of the Rh_2^{5+} complex, independent of isomer type.

Summary

In the present study, we have examined the structural, spectroscopic, and electrochemical properties of a series of dirhodium complexes bridged by four "anilinopyridinate-type" anions with fluorine atoms at the ortho, meta, or para positions of the phenyl ring. Both the isomer type, i.e., (4,0) or (3,1), and number of geometric isomers (one or two) vary with the nature of the bridging ligand. As is the case for the Ru_2^{5+} derivatives with similar bridging ligands, only the Rh_2^{5+} complexes with two substituents at the ortho positions of the phenyl group exist in two isomeric forms. No significant changes are observed in structural features upon increasing the number of F groups from 1 to 5, and whichever isomer effect is observed on the $M_2(L)_4$ framework of the Ru_2^{5+} derivatives with this type of bridging ligand, it is also seen for the Rh_2^{5+} derivatives, thus suggesting that the isomer effect on the structure does not appear to be influenced by the dimetal core, i.e., Ru_2 or Rh_2.

ESR and magnetic data of the seven investigated $Rh_2(L)_4Cl$ compounds indicate the existence of a single unpaired electron localized on one rhodium ion, independent of the isomer type or ligand basicity. Three of the investigated compounds undergo a single one-electron oxidation and a single one-electron reduction while four of the compounds undergo two one-electron oxidations and a single one-electron reduction in CH_2Cl_2, 0.1 M TBAP. The oxidations and reductions both follow linear free energy relationships between $E_{1/2}$ and the Hammett parameter of the substituents on the bridging ligand. The (4,0) and (3,1) isomeric forms of $Rh_2(2,6\text{-}F_2ap)_4Cl$ exhibit different UV−visible features as do the two isomers of $Rh_2(2,4,6\text{-}F_3ap)_4Cl$ and $Rh_2(F_5ap)_4Cl$.

Acknowledgment. The support of the Robert A. Welch Foundation (J.L.B., Grant E-918; K.M.K., Grant E-680) is gratefully acknowledged. We thank Dr. J. D. Korp for performing the X-ray analysis.

Supporting Information Available: X-ray crystallographic files in CIF format for the structural determination of $Rh_2(2\text{-}Fap)_4Cl$ (**1**), (4,0) $Rh_2(2,6\text{-}F_2ap)_4Cl$ (**2**), (3,1) $Rh_2(2,6\text{-}F_2ap)_4Cl$ (**3**), $Rh_2(F_5ap)_4Cl$ (**7**), $Rh_2(2,6\text{-}F_2ap)_4CN$ (**8**), and $Rh_2(2,4,6\text{-}F_3ap)_4(C{\equiv}C)_2Si(CH_3)_3$ (**9**). Table S1 lists the ESR, electrochemical, and spectroscopic data of (4,0) isomer $Rh_2(2,4,6\text{-}F_3ap)_4Cl$ (**4**), (4,0) $Rh_2(2,4,6\text{-}F_3ap)_4(C{\equiv}C)_2Si(CH_3)_3$ (**9**), and (3,1) isomer $Rh_2(2,6\text{-}F_2ap)_4Cl$ (**3**), $Rh_2(2,6\text{-}F_2ap)_4CN$ (**8**). Figures S1 and S2 (in PDF files) illustrate the ESR spectra of the (4,0) and (3,1) isomers of $Rh_2(L)_4Cl$, respectively. This material is available free of charge via the Internet at http://pubs.acs.org.

IC034963L